Extraction of Geopotential Height and Temperature Structure from Profiler and Rawinsonde Winds

STEVEN BUSINGER

Department of Meteorology, University of Hawaii, Honolulu, Hawaii

MICHAEL E. ADAMS,* STEVEN E. KOCH+ AND MICHAEL L. KAPLAN

North Carolina State University, Raleigh, North Carolina

(Manuscript received 11 April 2000, in final form 1 October 2000)

ABSTRACT

Mesoscale height and temperature fields can be extracted from the observed wind field by making use of the full divergence equation. Mass changes associated with irrotational ageostrophic motions are retained for a nearly complete description of the height field. Above the boundary layer, in the absence of friction, the divergence equation includes terms composed of the components of the wind and a Laplacian of the geopotential height field. Once the mass field is determined, the thermal structure is obtained through application of the hypsometric equation.

In this paper an error analysis of this *divergence method* is undertaken to estimate the potential magnitude of errors associated with random errors in the wind data. Previous applications of the divergence method have been refined in the following ways. (i) The domain over which the method is applied is expanded to encompass the entire STORM-FEST domain. (ii) Wind data from 23 profiler and 38 rawinsonde sites are combined in the analysis. (iii) Observed profiler and rawinsonde data are interpolated to grid points through a modified objective analysis, and (iv) the variation in elevation of the profiler sites is taken into account.

The results of the application of the divergence method to the combined wind data from profiler and rawinsonde sites show good agreement between the retrieved heights and temperatures and the observed values at rawinsonde sites. Standard deviations of the difference between the retrieved and observed data lie well within the precision of the rawinsonde instruments. The difference field shows features whose magnitude is significantly larger than the errors predicted by the error analysis, and these features are systematic rather than random in nature, suggesting that the retrieved fields are able to resolve mesoscale signatures not fully captured by the rawinsonde data alone.

The divergence method is also applied solely to the profiler data to demonstrate the potential of the divergence method to provide mass and thermal fields on a routine basis at synoptic times when operational rawinsonde data are not available. A comparison of the heights derived from the profiler winds with those independently measured by rawinsondes indicates that valuable information on the evolution of atmospheric height and temperature fields can be retrieved between conventional rawinsonde release times through application of the divergence method. The implications of the results for applications of the method in weather analysis and in numerical weather prediction are discussed.

1. Introduction

The installation of the National Oceanic and Atmospheric Administration's (NOAA) Profiler Network over the central plains provides meteorologists the opportunity to detect temporal features down to the mesoalpha and even mesobeta scale. Six-minute samples and hourly consensus averaging of wind profiles constitute a valuable dataset with which to identify and understand phenomena such as gravity waves, convective systems, frontal structure, and jet streak evolution (e.g., Zamora et al. 1987; Carlson and Forbes 1989; Bluestein and Speheger 1995; Ralph et al. 1995; Trexler and Koch 2000).

As a result of the prohibitive cost of asynoptic radiosonde releases, there remains a lack of observational data with which to resolve the temperature and mass fields needed for a complete thermodynamic description of mesoscale systems. Data from Aeronautical Radio, Incorporated, Communication, Addressing and Reporting System (ACARS), Radio–Acoustic Sounding System (RASS), and satellite-based sounders are helping reduce this deficiency. However, the distribution of

* Current affiliation: Air Force Weather Agency OL-H, Hanscom AFB, Massachusetts.

+ Current affiliation: NOAA-FSL, Boulder, Colorado.

Corresponding author address: Steven Businger, Department of Meteorology, University of Hawaii, 2525 Correa Rd., Honolulu, HI 96822.
E-mail: businger@soest.hawaii.edu

ACARS data is irregular in space and time, notably below normal jet aircraft cruising levels. RASS is limited to lower-tropospheric levels [<3.5 km above ground level (AGL)], and satellite retrievals are method/first guess dependent (Stankov 1998). Alternatively, the mesoscale mass and thermal structure for a region of the atmosphere can be retrieved through knowledge of the wind field, such as from a network of wind profilers, and application of the divergence equation (Fankhauser 1974; Kuo and Anthes 1985; Kuo et al. 1987a,b; Modica and Warner 1987; Gal-Chen 1988; Cram et al. 1991; Karyampudi et al. 1995).

Inspection of the full divergence equation reveals terms composed of the components of the wind and a Laplacian of the geopotential height field. An approximate solution to the Laplacian term can be obtained by employing the Liebmann overrelaxation method (Haltiner and Williams 1980), allowing the mass structure to be obtained from knowledge of the momentum field. The thermal structure is then derived using the hypsometric equation. An advantage of this *divergence method* is that it uses the total wind field including its rotational and irrotational components. Limiting assumptions concerning a balance between the mass and momentum fields through either semi- or quasigeostrophic assumptions are not necessary since the total derivative of the divergence field is retained. Consequently, mass changes induced by ageostrophic motions are preserved in the retrieved mass field.[1]

Previously, researchers have derived the height field from the wind field using select terms of the divergence equation in concert with either model-generated wind profiles or a limited mesoscale network of rawinsondes. Fankhauser (1974) employed the full divergence equation to generate a height field, using a mesoscale network of rawinsonde observations and no profiler data. Bleck et al. (1984) were the first to examine the potential for using wind profiler data to retrieve the height and temperature fields, but they chose to use the nonlinear balance equation because their interest was in large-scale phenomena. Gal-Chen (1988) conducted a detailed scale analysis of the full divergence equation and argued that the vertical motion terms are relatively unimportant for ''front like'' two-dimensional systems. However, Kuo and Anthes (1985) and Modica and Warner (1987) applied various forms of the divergence equation to determine model sensitivity in retrieving the mass structure. Both studies used model-generated wind profiles in constructing the mass field and verified the extracted mass field against the model. Not surprisingly, their efforts showed that errors were reduced when the divergence and vertical motion terms were included with the balance equation to form the complete divergence equation. This improvement can be attributed in part to the ability of the full divergence equation to describe dynamics associated with disturbances that are of sub-Rossby radius. Using model-generated datasets, Kuo et al. (1987a,b) applied the full divergence equation in a terrain-following σ-coordinate system. The results were quite sensitive to applied boundary conditions, with the use of Dirichlet boundary conditions providing the least error in the retrieved fields.

Cram et al. (1991) were the first to attempt to apply the divergence method to actual, as opposed to simulated, wind profiler observations. Their use of a small network of four profilers located in northeast Colorado produced a retrieved height field that was able to resolve a mesoscale trough that had gone undetected by the standard synoptic network. However, direct verification of the accuracy of the generated fields was not possible with just four profilers; thus, model output and other data sources were used to infer the accuracy of the results. Karyampudi et al. (1995) extended the work of Cram et al. (1991) in computing various kinematic diagnostics to identify a variety of mesoscale features. The fields were generated using the same approach employed by Cram et al. (1991) except the vertical motion fields were derived kinematically using an O'Brien (1970) adjustment technique to minimize the accumulation of errors, which assumes that the error variance is a linear function of height. The derived fields were then verified against the linear vector point function method of Zamora et al. (1987). Their efforts were successful in identifying the signature of a mountain wave, unbalanced upper-level frontogenesis, and a mesoscale tropopause fold coupled to the developing frontogenesis at midlevels.

The goal of this paper is to demonstrate the utility of the divergence method in weather analysis and to promote future applications and improvements of the method. Previous applications of the divergence method are refined by adapting it for the first time to a large (synoptic) domain containing a mesoscale network of rawinsondes during the Storm-scale Operational and Research Meteorology-Fronts Experiment System Test (STORM-FEST). This field experiment was held during the winter of 1992 in the central United States (Szoke et al. 1994) and benefits from abundant wind profiler and rawinsonde data. The availability of asynoptic rawinsonde observations from the STORM-FEST network provides a special opportunity to make direct comparisons between the mass and temperature fields sampled by the rawinsondes with those derived through the divergence method. Additionally, an error analysis is undertaken to estimate the impact of random errors on the accuracy of the method presented in this paper.

The approach developed by Cram et al. (1991) and Karyampudi et al. (1995) was modified in the following ways. (i) The domain over which the method was applied was expanded to include the entire STORM-FEST domain (Fig. 1) and (ii) a blended set of wind data from 23 profiler sites and from 38 rawinsonde sites were included in the analysis. (iii) Observed profiler and ra-

[1] In this paper the term *mass field* is used to refer to the integrated hydrostatic pressure field, which implicitly includes density and temperature.

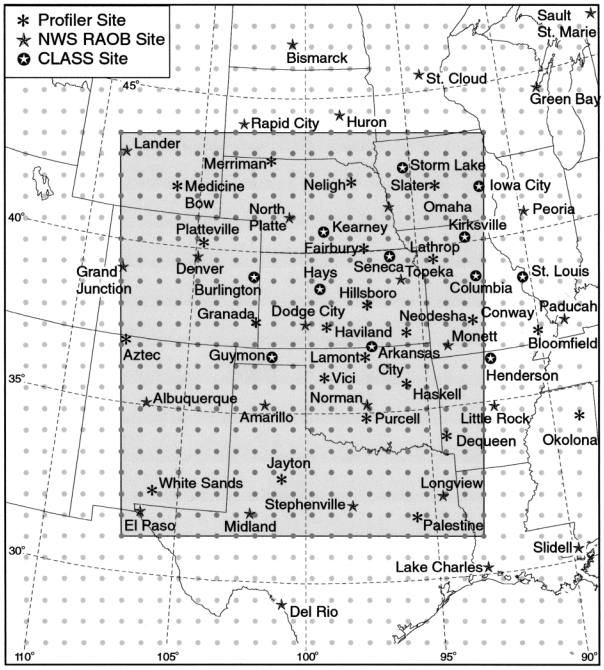

FIG. 1. Domain of objective analyses, showing location of upper-air observations. Dataset includes 23 profiler sites (asterisks), 26 National Weather Serivce (NWS) rawinsonde sites (stars), and 12 National Center for Atmospheric Research (NCAR) CLASS sites (circled stars). Objective analysis scheme is based upon a grid spacing of 85 km. Shaded region depicts primary 20 × 20 grid domain. The outer 30 × 30 grid is used to assist in the analysis along the boundary of the primary domain.

winsonde data were interpolated to a grid through a modified objective analysis, and (iv) the variation in elevation of the profiler sites is taken into account. Constrained kinematic vertical motion was used in the divergence equation to minimize the impact of subgrid-scale vertical motions and contamination of the vertical beam data during precipitation.

Two applications of the divergence method are presented in this paper. First, the 3-hourly STORM-FEST rawinsonde wind observations are used in combination with the profiler wind data to retrieve the mass and thermal fields for application in case-study analyses (section 4). This work was undertaken as part of an investigation of the generation and propagation of a cold front aloft in the lee of the Rocky Mountains (Locatelli et al. 1995). Second, the heights derived from profiler winds using rawinsonde data as boundary conditions are compared with heights derived from rawinsonde observations in a test of the potential for the divergence method to provide asynoptic data on a routine basis from the profiler network (section 5). Potential future improvements and applications of the method are discussed.

2. Data and methodology

The NOAA 404-MHz profilers installed over the central plains consist of a ground-based Doppler radar with a three-beam antenna field (Strauch et al. 1987). The geometry of the system consists of a vertically oriented antenna and two other antennas directed in the north–south and east–west plane, respectively, and offset from the zenith by an angle of 16.3°, thus providing in situ measurements of the u, v, and w components of the momentum field. The vertical beam detects the vertical motion field in the absence of precipitation, while the north and east pointing beams measure off-zenith radial velocities. Based upon Doppler principles, each antenna successively emits a pulse and then detects the backscattered energy returned to the sensor. Radial velocities are measured in two different height modes on the three antenna beams, giving six different combinations that each take 1 min. Thus, radial velocities on any given beam/mode are sampled every 6 min. These samples are averaged over an hour to provide a consensus averaged wind observation.

An extended comparison between profiler and rawinsonde winds shows a standard deviation of 2.5 m s^{-1} (Weber and Wuertz 1990). Detailed analyses with a different dataset show the horizontal wind components to be within ±1 m s^{-1} of rawinsonde values at all levels (Strauch et al. 1987; May and Strauch 1989).

The three-beam profiler data during STORM-FEST were processed using the NOAA Weber–Wurtz quality control algorithm designed to eliminate contamination resulting from lack of backscatter, birds and insects, etc. When precipitation is highly inhomogeneous, as in convective rain events, the horizontal profiler winds can become contaminated by noise introduced by falling precipitation (Ralph et al. 1995). Therefore, data used in this study were visually checked for spatial and temporal consistency. When a particular wind barb shows a discrepancy with wind barbs on either side, vertically or temporally, the data point is replaced with a weighted average of the adjacent wind barbs (weighting applied: 75% vertical, 25% temporal). The discrepancy criteria are gate-to-gate differences in wind direction exceeding 55° and/or gate-to-gate differences in wind speed exceeding 35 m s^{-1}.

Depending on the availability of atmospheric scatterers and weather conditions, the NOAA profilers can sample the atmosphere from 0.5 to 16 km at a vertical resolution of 250 m (below 9 km) and 1 km (at higher levels). Therefore profiler wind data are not available at altitudes below approximately the 850-mb level over the western plains.

In this study, direct measurements of vertical velocity from the profiler sites were used in calculation of horizontal winds. However, kinematic vertical velocities, rather than vertical beam data, are used in additional diagnostic analysis. By calculating vertical motion from the horizontal winds, some smoothing is undertaken, but the smoothing is consistent with the scale being analyzed and reduces noise introduced by subgrid-scale up- and downdrafts and contamination of vertical beam data during precipitation events. Moreover, this approach is

consistent with the fact that rawinsonde data do not provide vertical wind data.

The mass and thermal structure of the atmosphere can be extracted from hourly profiler data through application of the full divergence equation. The divergence equation in pressure coordinates can be written (e.g., Fankhauser 1974)

$$-\nabla^2\phi = \underset{\text{A}}{} -f\left(\frac{\partial v}{\partial y} - \frac{\partial u}{\partial x}\right) \underset{\text{B}}{} - 2\underset{\text{C}}{\left(\frac{\partial v}{\partial x}\frac{\partial u}{\partial y} - \frac{\partial u}{\partial x}\frac{\partial v}{\partial y}\right)}$$

$$+ \underset{\text{D}}{\beta u} + \underset{\text{E}}{\left(\frac{\partial \omega}{\partial x}\frac{\partial u}{\partial p} + \frac{\partial \omega}{\partial y}\frac{\partial v}{\partial p}\right)} + \underset{\text{F}}{D^2}$$

$$+ \underset{\text{G}}{\left(\frac{\partial D}{\partial t} + u\frac{\partial D}{\partial x} + v\frac{\partial D}{\partial y} + \omega\frac{\partial D}{\partial p}\right)}$$

$$+ \underset{\text{H}}{\left(\frac{\partial F_u}{\partial x} + \frac{\partial F_v}{\partial y}\right)}, \qquad (1)$$

where D is the horizontal two-dimensional velocity divergence; u, v, and ω are the components of the total wind V; f is the Coriolis parameter; β is the meridional variation of f; ϕ is the geopotential height; and F represents the frictional contribution. Terms A–D in (1) represent the balance equation (Haltiner and Williams 1980).

The divergence method was applied during STORM-FEST Intensive Operation Period-17 (IOP-17; 8–9 Mar 1992), a period rich in upper-air data. In order to accommodate the nonuniform distribution of the combined rawinsonde–profiler sites (mean spacing $\Delta n \sim$ 128 km) and the rawinsonde sites alone, a grid spacing of 85 km was selected (Fig. 1). The analysis grid spacing was chosen small enough to be able to fully represent the $4\Delta n$ waves, while maintaining the resolution inherent in the observations (Koch et al. 1983). In the vertical, the objective analysis was constructed at nine levels (850, 800, 700, 600, 500, 400, 300, 200, and 100 mb).

Profiler winds are only available on height levels at 250-m increments. Consequently, the profiler winds must be interpolated to pressure levels. This is accomplished using the pressure–height information from the rawinsonde data. In the absence of sounding data, a gridded analysis of the rawinsonde data for two time periods is required to arrive at a time-interpolated mass field, which is then used to convert the altitude of the profiler winds to the corresponding pressure level. This circumstance is explored further in section 5. For the case of a combined dataset, a two-pass Barnes objective analysis (Koch et al. 1983) of the rawinsonde heights is conducted for a given pressure level. Then a bilinear interpolation is performed between grid points and the profiler locations to establish the height of the specified pressure level at the profiler sites. Next a vertical linear interpolation of the profiler wind data from adjacent levels in the vertical is performed to obtain the appropriate horizontal wind components for the given pressure level. Finally, a two-pass Barnes analysis of the combined rawinsonde and profiler winds is conducted to obtain a gridded wind field for each pressure level.

Once the combined wind field is available, the initial step in retrieving the mass field from the full divergence equation is to generate fields of two-dimensional horizontal divergence and kinematic vertical motion from the horizontal wind field for a given pressure level. The horizontal divergence and vertical motions are determined through second-order centered finite-difference calculations using gridded datasets. This simplifies the computation of the divergence field but is susceptible to error. As mentioned previously, the data were carefully quality controlled to ensure that the wind profiles did not contain erroneous wind speeds or directions.

The kinematic vertical motion field is determined by vertically integrating the horizontal divergence, under the assumption that the vertical motion of the lowest layer is zero. An O'Brien (1970) adjustment technique was employed to minimize the accumulation of errors as divergence is vertically integrated to the top of the domain at the 100-mb level. The technique employed assumes that the error variance is a linear function of height. It is conceded that the absence of winds below ~0.5 km in the profiler winds used here may have decreased the accuracy of the final kinematic velocity calculations. However, the advantage of this approach is that the method relies only on the availability of profiler wind data.

The frictional terms of the divergence equation (1) are neglected under the assumption that such effects are minimal in the free atmosphere (above 850 mb), away from strong upper-level fronts. This assumption could have its greatest impact in the lowest levels, as divergence calculations are not influenced by the momentum fluxes experienced in the convective boundary layer (Karyampudi et al. 1995). Equation (1), derived for a Lambert conformal map projection, can then be expressed

$$F = -m^2\nabla^2\Phi$$

$$= \frac{\partial D'}{\partial t} + m^2\left(u\frac{\partial D'}{\partial x} + v\frac{\partial D'}{\partial y}\right) + m^2(D')^2$$

$$+ 2m^2\left(\frac{\partial v}{\partial x}\frac{\partial u}{\partial y} - \frac{\partial u}{\partial x}\frac{\partial v}{\partial y}\right) + \omega\frac{\partial D'}{\partial p}$$

$$+ m\left(\frac{\partial \omega}{\partial x}\frac{\partial u}{\partial p} - \frac{\partial \omega}{\partial y}\frac{\partial v}{\partial p}\right) - m\gamma v + m\beta u - f\zeta, \qquad (2)$$

where m is the map factor, and $D' = m^2\nabla \cdot \mathbf{V}/m$, and F denotes the sum of the forcing terms (Kuo and Anthes 1985). The individual terms of the forcing function can

be solved from the analyzed wind field based on the rawinsonde and profiler data. Consequently, by employing the Liebmann overrelaxation method, an approximate numerical solution to the Laplacian function can be obtained, yielding the geopotential height field. The rawinsonde-generated height fields are used as the first guess and provide the necessary Dirichlet boundary conditions for the grid, while the calculated forcing function values make up the interior portion of the domain.

Once the height field is generated, the thermal structure is computed by assuming hydrostatic balance and making use of the hypsometric equation,

$$\phi(z_u) - \phi(z_l) = R \int_{P_u}^{P_l} T_v d \ln p, \tag{3}$$

where R is the universal gas constant and T_v is the virtual temperature. Virtual temperatures are calculated for the layer between the input heights and assumed valid at the midpoint pressure of the layer. They are then interpolated logarithmically with respect to pressure back to the original pressure levels.

3. Error analysis of the profiler thermodynamic retrieval

There are several sources of potential error in the mass retrieval techniques presented in section 2: (i) systematic biases in profiler measurements, (ii) the objective analysis of the profiler and rawinsonde data, (iii) truncation errors in calculating spatial and temporal derivatives, and (iv) random profiler measurement errors. The error analysis presented here treats only the impact of the random errors for the following reasons. First, Martner et al. (1993) found that mean differences (bias) between 404-MHz profilers and collocated rawinsondes was only $\sim$0.6 m s^{-1}. Regarding the objective analysis error component, the use of the linear vector point function (LVPF) technique to compute divergence from an array of profilers by Zamora et al. (1994) produced divergence error $\partial_\varepsilon < 10\%$ as long as the grid size was smaller than one-fourth of the wavelength ($\Delta x/\lambda < 0.25$). For the scale of features with which we are concerned $\Delta x/\lambda < 0.1$, see Fig. 4), the error is negligible ($\partial_\varepsilon < 2\%$). Thus, analysis error can be safely ignored provided that the Barnes objective analysis produces errors equivalent to those of the LVPF, which is suggested by the results of Karyampudi et al. (1995). We do not specifically treat truncation errors in the analysis, but they are presumed to be of secondary importance.

The remaining error is that of random measurement errors. Detailed analyses by May and Strauch (1989) and Strauch et al. (1987) show the horizontal wind components to be within ± 1 m s^{-1}. Kuo and Anthes (1985) assumed rmse = 1 m s^{-1} using 12-hourly model data on a 350-km grid mesh. Therefore, we have assumed that profiler rmse = 1.0 m s^{-1} in this error analysis. Additionally, the following assumptions are used in the error analysis: (i) the effects of friction are ignored, (ii) the scale over which random errors occur is the grid spacing of 85 km, (iii) wind component rmse = $|\delta u| = |\delta v| = 0.7$ m s^{-1} = 5% (given $|\delta V| = 1$ m s^{-1} and mean wind of 28 m s^{-1}), and (vi) profiler and rawinsonde sampling time of $\Delta t = 3$ h.

Employing the assumptions outlined above and assuming centered differences results in a total error of 13.01×10^{-9} s^{-2} (details are given in the appendix). This can be considered as an error forcing function for the Laplacian of height, from which we arrive at the resultant retrieved height error of 19 m. This result is consistent with the fact that the height-dependent standard deviation of the difference between our retrieved height field and that observed by the 12-hourly rawinsondes varied from 8 to 14 m. The estimated retrieved height error of 19 m is also comparable to other findings. Kuo and Anthes (1985) obtained a 19-m height error using 12-hourly data from the Second European Stratospheric Arctic and Mid-latitude Experiment (SESAME) on a 360-km grid mesh. Kuo and Anthes (1985) obtained 4.0-m height error using 3-hourly SESAME data on a 360-km grid mesh. Kuo et al. (1987a) obtained a 6-m height error using 1-hourly data on a 350-km grid mesh, and a 9-m height error using 1-hourly data on a 40-km grid mesh.

4. Results of the divergence method using all available wind data

The application of the divergence method using all available wind data in the STORM-FEST dataset and comparing the results to radiosonde data is provided as an example of the application of the approach. The 500-mb height fields, derived using combined wind data, document the evolution of an approaching upper-level low over the Front Range of the Rocky Mountains (Fig. 2). A developing trough over the inner-mountain region at 2100 UTC 8 March 1992 is captured (Fig. 2a), and a building ridge over the central plains is consistent with the anticyclonic flow over this region. By 0300 UTC 9 March 1992, the trough has deepened significantly over the New Mexico–Colorado border, where 6-h height falls exceed 60 m (Fig. 2b). The retrieved height field at 0300 UTC shows height falls of only 25–30 m over southwestern Oklahoma, tightening the height gradient over the Texas panhandle. To the east an elongated trough extending from central Oklahoma to northeastern Texas is detected. This feature is aligned with an area of convective precipitation over eastern Oklahoma (Fig. 3).

Figure 4 shows the difference between the retrieved height field and the rawinsonde-derived height field.[2] A

[2] The difference fields in Fig. 4 were generated through objective analysis of the gridded datasets, whereas the numbers plotted in Fig. 2 are the differences at the sites. Therefore, the contour values in Fig. 4 may deviate slightly from the plotted numbers.

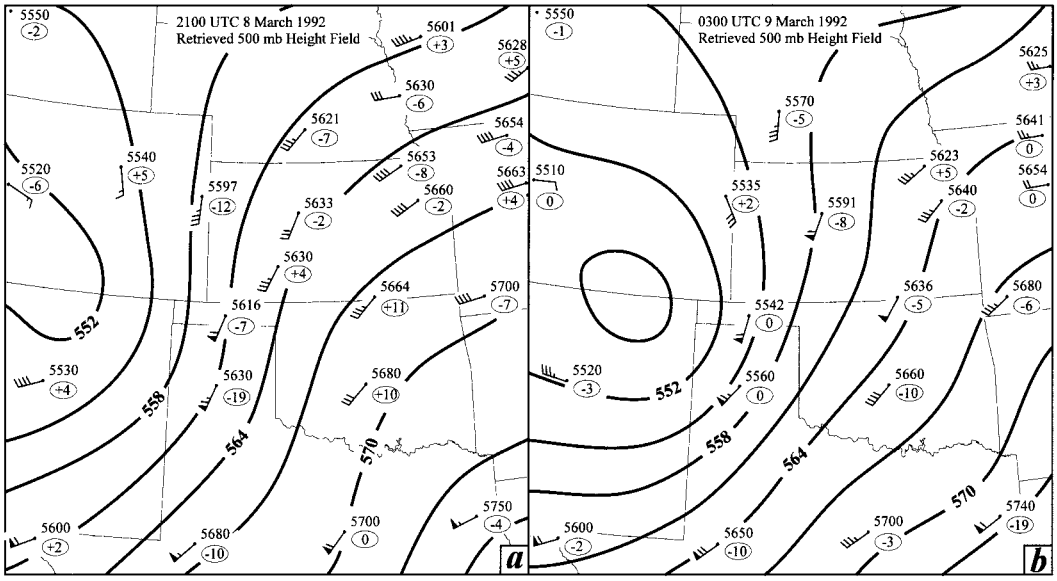

FIG. 2. Retrieved 500-mb geopotential height field (every 30 m) for (a) 2100 UTC 8 Mar 1992 and (b) 0300 UTC 9 Mar 1992. Station plots show the observed heights (m) and wind barbs (flag − 25 m s^{-1}; full staff − 5 m s^{-1}; half staff − 2.5 m s^{-1}) from the NWS rawinsonde and NCAR CLASS soundings. The encircled number plotted below each height value is the difference between the retrieved and observed height. Negative value indicates retrieved mass field is lower than observed field.

coherent pattern emerges that can be attributed to the impact of the profiler data on the analysis. The developing low over the Front Range is significantly deeper than that objectively analyzed with rawinsonde data alone. Additionally, the mesoscale tendency for ridging over southwestern Oklahoma and the eastern Texas panhandle and the elongated trough extending from central Oklahoma to northeastern Texas are more pronounced than in the rawinsonde analysis.

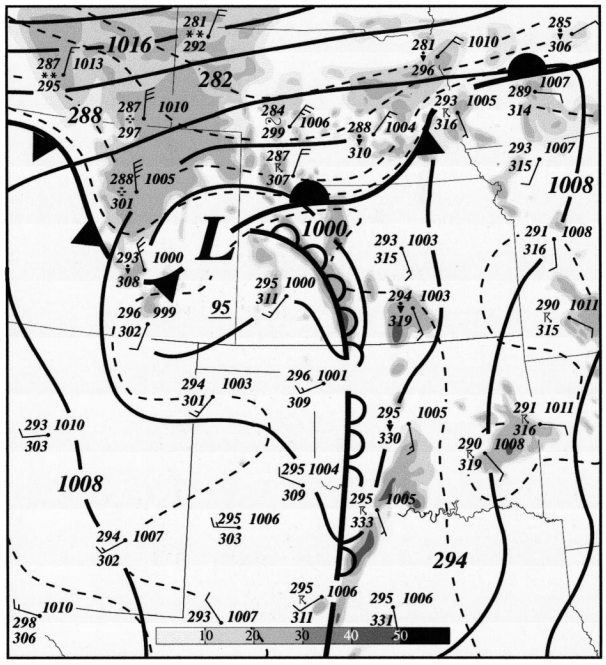

FIG. 3. Surface analysis for 0300 UTC 9 Mar 1992, showing isobars (every 4 mb), theta (dashed, K), and radar reflectivity (shading every 10 dBZ). Station plots include theta, theta-e, mean sea level pressure, observed weather, and winds (standard convention).

The extracted heights compare well with observed rawinsonde heights (Fig. 2). The differences between the retrieved and observed heights at the rawinsonde sites are well within the measurement errors associated with the sounding systems [±24 m; Hoehne (1980)]. The signals seen in Fig. 4 are significantly above the noise level associated with the method as diagnosed by the error analysis presented in the section 3. Therefore, the systematic differences seen in Fig. 4 represent a real impact of the profiler data in the analysis.

Standard deviations of the difference data were calculated as an additional check for the accuracy of the method. At 2100 UTC the height differences have a standard deviation of ±7 m, with the retrieved heights showing slightly lower values than those observed on average. At 0300 UTC, the standard deviation is ±5 m. The standard deviations of the height differences for five times and at four levels all fall within the accuracy of the rawinsonde observations (Table 1). The smallest deviations are seen at lower atmospheric levels and the deviations increase at higher levels. These statistics are consistent with the error analysis and the findings of Kuo et al. (1987a) and Kuo and Anthes (1985).

Investigation of the corresponding temperature differences reveals similar results to those obtained for the height data (Table 1). Although an analytical error analysis was not undertaken for the retrieved temperatures,

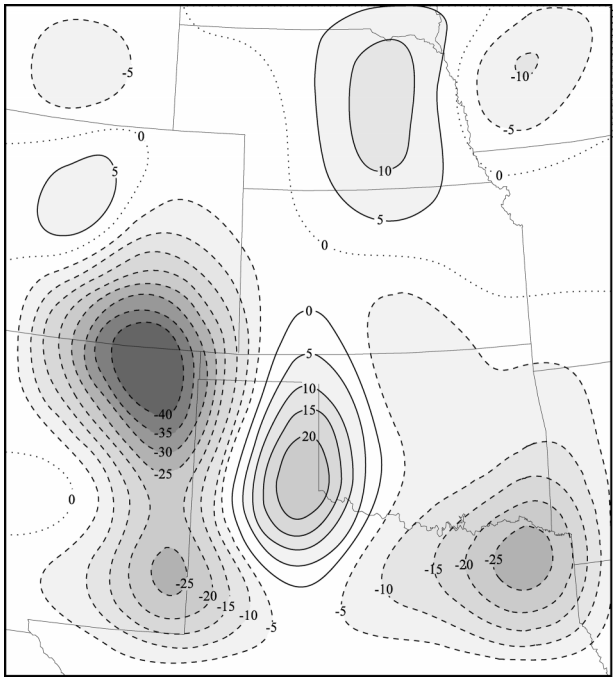

FIG. 4. Retrieved height field minus the rawinsonde derived height field (contours every 5 m) at the 500-mb level for 0300 UTC 9 Mar 1992. Dashed lines indicate negative values and solid lines indicate positive values. Successively greater differences between the fields are shaded accordingly.

they are generally within 1°–2°C of the observed values. This result compares well with the results by Kuo and Anthes (1985) who found rms errors of 1.55° for model-generated fields subjected to random errors representative of observed conditions. The temperature deviations (Table 1) again show that the errors increase with elevation.

Figure 5 compares two retrieved thermal profiles with the corresponding observed STORM-FEST Cross-chain Linked Atmospheric Sounding System (CLASS) sounding at Guymon, Oklahoma (GUY in Fig. 1). Since the vertical resolution of the extracted temperature field is limited to 100-mb intervals above 800 mb, a reproduction of the detailed structure of the observed temperature profile is not expected. However, the retrieved temperatures match those observed very well at the levels where the retrieval was undertaken, with all the significant differences existing between these levels, supporting the potential utility of the method. The cooling trend at all levels below 400 mb, with a maximum near 500 mb is correctly captured by the derived temperature profiles. The enhanced midlevel cooling is associated with a developing cold front aloft, a feature that was analyzed by Locatelli et al. (1995).

The standard deviation between the derived and observed temperature profiles is ±0.79°C at 2100 UTC and ±0.42°C at 0300 UTC. As previously noted, the retrieved sounding did not capture the vertical structure of the rawinsonde sounding because of the lack of vertical resolution in the retrieved data. Applying the method at all levels for which profiler data are available would increase the vertical resolution and the potential utility of the retrieved data for assessing the stability of the atmosphere.

5. Divergence method using profiler winds at asynoptic times

Since the profiler network provides a reliable source of wind data at hourly intervals, it is useful to demonstrate the potential of the divergence method to provide mass and thermal fields on a routine basis at asynoptic times when operational rawinsonde data are not available. In the absence of sounding data, a gridded analysis of the rawinsonde data for two time periods is required to arrive at a time-interpolated mass field, which is then used to convert the altitude of the profiler winds to the corresponding pressure level. A linear time interpolation is applied to generate a rawinsonde mass field that corresponds in time to the observed profiler data. Operationally, 12-hourly synoptic rawinsonde observations must be used for this purpose. Dirichlet boundary conditions used to invert the profiler wind data were also obtained from 12-hourly synoptic sounding data through linear interpolation in time. Another approach, in the absence of sounding data, is to use NWP model output for boundary conditions at the asynoptic times.

The height field derived from the enhanced STORM-FEST rawinsonde dataset is used as a conservative standard for comparison in Fig. 6. The results show that the height field extracted from the profiler winds is comparable to the height field objectively analyzed from rawinsonde data (Fig 6). The extracted height field successfully captures the overall pattern of a deepening

TABLE 1. Standard deviation (σ) of the difference between the retrieved height (m)/temperature (°C) field and the observed height/temperature field from rawinsondes over a 12-h period centered at 0000 UTC 9 Mar 1992.

	Time (UTC)					
Level (mb)	1800	2100	0000	0300	0600	Mean σ
700	7 m/1.5°	5 m/1.3°	7 m/1.3°	13 m/1.9°	14 m/1.5°	9 m/1.5°
500	8 m/1.2°	7 m/0.9°	10 m/1.1°	5 m/1.4°	10 m/1.2°	8 m/1.1°
400	9 m/1.0°	13 m/1.3°	10 m/1.1°	7 m/1.3°	11 m/1.2°	10 m/1.2°
300	13 m/1.9°	12 m/2.3°	16 m/2.4°	13 m/1.9°	17 m/1.5°	14 m/2.0°

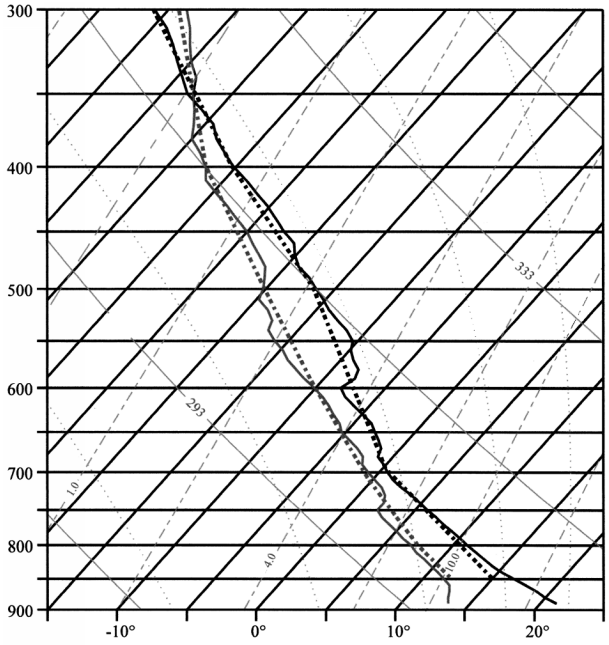

FIG. 5. Standard skew *T* plot of derived (heavy dashed lines) and observed (heavy solid lines) temperature profiles for Guymon, OK. Temperature profiles for 2100 UTC 8 Mar 1992 are depicted in gray and temperature profiles for 0300 UTC 9 Mar 1992 are depicted in black.

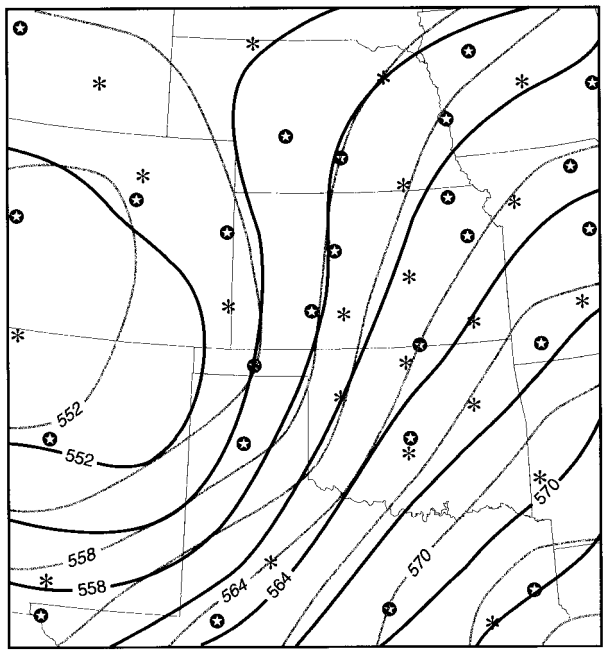

FIG. 6. Analysis of 500-mb height field (every 30 m) for 0300 UTC 9 Mar 1992. Heavy black lines depict heights derived from profiler winds and heavy gray lines depict height field obtained from rawinsonde observations. Asterisks indicate locations of profiler sites and stars indicate rawinsonde sites.

trough over the high plains with a ridge over the Midwest. The trough is slightly stronger over New Mexico and the downstream ridge over eastern Nebraska and Kansas is weaker in the extracted height analysis.

6. Discussion and conclusions

Enhanced rawinsonde observations from the STORM-FEST field experiment provide an opportunity in which to review and refine a method, based on application of the divergence equation, to extract a geopotential height and thermal structure from observed wind data. By making use of the full divergence equation, the mesoscale height field can be extracted from the observed wind field. Mass changes associated with irrotational ageostrophic motions are retained for a nearly complete description of the height field. Above the boundary layer, in the absence of friction, the divergence equation includes terms composed of the components of the wind and a Laplacian of the geopotential height field. Once the mass field is determined, the thermal structure is obtained through application of the hypsometric equation.

The goal of this paper is to demonstrate the utility of the divergence method in weather analysis and to promote future applications and improvements of the method. The mass retrieval approach developed by Cram et al. (1991) and Karyampudi et al. (1995) was modified in the following ways. The data domain was expanded to include 3-hourly rawinsonde and NOAA profiler sites within the STORM-FEST domain. The interpolation of the combined wind data to grid points was accomplished through application of objective analysis methods. And the variation in elevation of the profiler sites was taken into account.

The divergence method was applied during STORM-FEST IOP-17 (8–9 Mar 1992), a field experiment rich in upper-air data. This IOP was characterized by an upper-level low that deepened in the lee of the Rockies and spawned a cold front aloft (CFA) and severe weather over the plains states (Locatelli et al. 1995).

The retrieved heights compared well with heights observed at rawinsonde sites (Table 1), with an average standard deviation of ± 10 m. Moreover, the results are consistent with the error analysis, suggesting that the retrieved fields are able to resolve coherent mesoscale features not fully captured by the rawinsonde data alone. Results of the comparison of retrieved and observed temperatures show retrieved temperatures were within ± 1.5°C of observed temperatures. Retrieved temperature soundings detected enhanced cooling at midtropospheric levels over the Texas panhandle region associated with passage of a developing CFA. The potential utility of retrieved temperature soundings for assessing the stability of the atmosphere will depend on the vertical resolution (100 mb in this case) of the data used in the retrieval.

The greatest accuracy for the retrieved height and temperature fields was obtained in the middle troposphere (700 and 500 mb). The decrease in accuracy at

higher tropospheric levels may be due to several factors. These include (i) a loss in representativeness of the upper-level rawinsonde observation as the balloon travels downwind, (ii) a smaller number of observations available at higher altitudes, (iii) a decrease in the accuracy of the kinematically computed vertical motion using upward integration, and (iv) the influence of stratospheric intrusions on the thermal structure in relation to the vertical resolution of the retrieval process.

Several suggestions have been made for improvements to the method described in this paper. The absence of profiler winds below ~0.5 km used in this study may have decreased the accuracy of the final kinematic velocity calculations. The advantage of this approach is that the method relies only on the availability of profiler wind data. Shaltanis (1998) modified the method described here to include friction in the retrieval process. He determined that the effects of frictional stresses on the retrieved mass field are small when the low-level flows are light to moderate. It should be noted that the divergence method can be applied to each level for which data are available. In the case of profiler observations, data are available at 250-m intervals and the method could help resolve significant features in the thermal profile of the atmosphere. The linear vector point function technique has been shown to reduce errors in calculating divergence (Zamora et al. 1987, 1994). Karyampudi et al. (1995) show that a Barnes objective analysis with an O'Brien adjustment, as used in the current study, applied to a small network of wind profilers produces statistically similar results to the LVPF method, even with high-level diagnostic fields. Nevertheless, future researchers are encouraged to explore an approach that incorporates LVPF.

This application of the divergence method using hourly profiler data provided encouraging results at asynoptic times when operational rawinsonde data are not available. The extracted height field successfully captured the overall synoptic pattern over the plains region, illustrating the ability of the divergence method to provide useful height information at times when rawinsonde observations may not be available. These results relied on profiler wind data, but the divergence method can be applied to wind data regardless of their source, including wind data derived from satellite (e.g., Nieman et al. 1993) and Doppler radar (e.g., Campistron et al. 1991).

The fact that useful information can be retrieved from wind data at asynoptic times suggests that an application of this technique to a combination of profiler, Weather Surveillance Radar-1988 Doppler radar, and satellite-derived wind data could provide valuable mass and thermal constraints for the update cycle of operational numerical models. Similarly the method could find application in the increasing number of regional mesoscale models run locally in a quasi-operational mode. Applications to numerical weather prediction initialization require significant additional research to dynamically assimilate time-continuous data and to compare the effectiveness of this approach to developing data assimilation schemes based on variational methods.

Acknowledgments. This research was supported by the United States Air Force through the Air Force Institute of Technology program. Special appreciation is given to Dr. Jennifer M. Cram (NCAR) for graciously providing the application code. Her assistance was invaluable in applying the divergence method to the STORM-FEST dataset. Appreciation is extended to Robert Rozumalski for his assistance in this effort by providing the means to convert the output for display and his assistance in modifying the retrieval code. The authors are grateful for constructive comments provided by three anonymous reviewers. This research was supported by the National Science Foundation under Grants ATM-9496335 and ATM-9700626.

APPENDIX

Profiler Thermodynamic Retrieval Error Analysis

Employing the assumptions discussed in section 3, the error contributed by each of the nine terms in the retrieval equation [Eq. (2)] was computed. A standard practice in error analysis is to rewrite an error term using fractional uncertainties. For example, consider the error due to measurement of horizontal divergence from a network of wind profilers. The scaled divergence, assuming centered finite differencing, is calculated as

$$D = \frac{\partial u}{\partial x} + \frac{\partial v}{\partial y} \approx \frac{u}{2\Delta x} = \frac{20 \text{ m s}^{-1}}{2 \times 85 \text{ km}} = 1.2 \times 10^{-4} \text{ s}^{-1}, \quad \text{(A1)}$$

and the divergence error as

$$\delta D \cong 2\delta\left(\frac{\partial u}{\partial x}\right) = 2\left[\frac{\partial}{\partial x}(\delta u)\right] = 2 \times \frac{0.7 \text{ m s}^{-1}}{2 \times 85 \text{ km}} = 8.2 \times 10^{-6} \text{ s}^{-1}. \quad \text{(A2)}$$

We also note for use in scaling analysis to follow that

$$\frac{\partial D}{\partial x} = \frac{1.2 \times 10^{-4} \text{ s}^{-1}}{2 \times 85 \text{ km}} = 7.1 \times 10^{-10} \text{ m}^{-1} \text{ s}^{-1}. \quad \text{(A3)}$$

Accordingly, the fractional uncertainties for the east–west wind component and divergence are $\delta u/u = 0.035$ (3.5%) and $\delta D/D = 0.069$ (6.9%), respectively. One may switch the order of differentiation, as was done above with the divergence error (A2). Errors arising from terms involving vertical motion were handled by assuming that the O'Brien scheme was effective at minimizing the vertical accumulation of errors arising from upward integration of horizontal divergence; hence, the integrated divergence errors were replaced with a constant, as follows. Since vertical motion is estimated as

$$\omega_i = \omega_{i-1} + \sum_{i'-1}^{N} D_{i'}\,dp, \tag{A4}$$

we replace the integrated divergence with a constant (δD), assuming the effectiveness of the O'Brien scheme, for purposes of scale analysis:

$$\omega\frac{\partial D}{\partial p} \cong \frac{\partial D}{\partial p}\sum D_i\Delta p \approx D^2,$$

$$\therefore\ \delta\left(\omega\frac{\partial D}{\partial p}\right) \approx \delta D^2 = 2D\delta D = 2.0\times 10^{-9}\ \mathrm{s}^{-2}. \tag{A5}$$

One must add all the separate components to arrive at the final error estimate in this case, because the individual contributing errors are not independent of one another. However, as shown below, the ''beta'' and ''gamma'' terms have negligible errors.

1) Error in divergence tendency term:

$$\delta\left(\frac{\partial D}{\partial t}\right) = \frac{\partial}{\partial t}(\delta D) = \frac{\delta D}{2\Delta t} = 0.38\times 10^{-9}\ \mathrm{s}^{-2}. \tag{A6}$$

Time interval (δt) used is 3 h.

2) Error in horizontal advection of divergence term:

$$\frac{\delta\left(u\frac{\partial D}{\partial x}+v\frac{\partial D}{\partial y}\right)}{\left|u\frac{\partial D}{\partial x}+v\frac{\partial D}{\partial y}\right|} \cong \frac{2\delta\left(u\frac{\partial D}{\partial x}\right)}{\left|u\frac{\partial D}{\partial x}\right|} = 2\left[\frac{\delta u}{|u|}+\frac{\frac{\partial}{\partial x}(\delta D)}{\frac{\partial D}{\partial x}}\right]$$

$$= 2\left(\frac{\delta u}{u}+\frac{\delta D}{D}\right) = 0.208$$

$$\therefore\ \delta\left(u\frac{\partial D}{\partial x}+v\frac{\partial D}{\partial y}\right) = 2\left(\frac{\delta u}{u}+\frac{\delta D}{D}\right) \times\left|u\frac{\partial D}{\partial x} = 2.95\times 10^{-9}\ \mathrm{s}^{-2}\right|. \tag{A7}$$

3) Error in nonlinear divergence term:

$$\delta D^2 = 2D\delta D = 1.97\times 10^{-9}\ \mathrm{s}^{-2}. \tag{A8}$$

4) Error in Jacobian term:

$$\delta\left(\frac{\partial v}{\partial x}\frac{\partial u}{\partial y}-\frac{\partial u}{\partial x}\frac{\partial v}{\partial y}\right) \cong 2\delta\left(\frac{\partial v}{\partial x}\frac{\partial u}{\partial y}\right) \cong 4\frac{\partial}{\partial x}(\delta v)\left|\frac{\partial v}{\partial x}\right|$$

$$= 1.97\times 10^{-9}\ \mathrm{s}^{-2}. \tag{A9}$$

5) Error in vertical advection of divergence term (see section 3):

$$\delta\left(\omega\frac{\partial D}{\partial p}\right) = \left[\frac{\delta\omega}{|\omega|}+\frac{\frac{\partial(\delta D)}{\partial p}}{\left|\frac{\partial D}{\partial p}\right|}\right]\left|\omega\frac{\partial D}{\partial p}\right| = 2D\delta D$$

$$= 1.97\times 10^{-9}\ \mathrm{s}^{-2}. \tag{A10}$$

6) Error in tilting term (see section 3):

$$\delta\left(\frac{\partial\omega}{\partial x}\frac{\partial u}{\partial p}-\frac{\partial\omega}{\partial y}\frac{\partial v}{\partial p}\right)$$

$$\approx 2\delta\left(\frac{\partial\omega}{\partial x}\frac{\partial u}{\partial p}\right) \cong 2\delta\left(\frac{\partial\omega}{\partial p}\frac{\partial u}{\partial x}\right) \cong 2\delta\left(D\frac{\partial u}{\partial x}\right)$$

$$= 2\left(\frac{\delta D}{|D|}+\frac{\delta D/2}{|D|}\right)|D^2| = 3D\delta D$$

$$= 2.95\times 10^{-9}\ \mathrm{s}^{-2}. \tag{A11}$$

7) Error in beta terms:

$$\delta(\gamma v) = \gamma\delta v = \frac{\partial f}{\partial x}\delta v \cong 0$$

$$\delta(\beta u) = \beta\delta u = 7\times 10^{-12}\ \mathrm{s}^{-2} \cong 0. \tag{A12}$$

8) Error in vorticity term:

$$\delta(f\zeta) = f\delta\left(\frac{\partial v}{\partial x}-\frac{\partial u}{\partial y}\right) \cong 2f\frac{\partial}{\partial x}(\delta v)$$

$$= 0.82\times 10^{-9}\ \mathrm{s}^{-2}. \tag{A13}$$

9) Friction ignored.

Summary of forcing terms errors:

$$\text{Total error}\ \sum_{i=1}^{9} F_i = 13.01\times 10^{-9}\ \mathrm{s}^{-2}. \tag{A14}$$

This error in the total forcing (A14) for determining the geopotential height results in a certain height retrieval error ($\delta\phi$). Given that

$$\delta(\nabla^2\phi) = \delta\left(\frac{\partial^2\phi}{\partial x^2}+\frac{\partial^2\phi}{\partial y^2}\right) \cong 2\delta\left(\frac{\partial^2\phi}{\partial x^2}\right), \tag{A15}$$

it follows that

$$\delta\phi = 2(\Delta x)^2\delta\left(\sum_{i=1}^{N} F_i\right)$$

$$= 2(85\times 10^3\ \mathrm{m})^2(13.01\times 10^{-9}\ \mathrm{s}^{-2})$$

$$= 188\ \mathrm{m}^2\ \mathrm{s}^{-2}. \tag{A16}$$

Hence, the estimated retrieved height error due to random errors is

$$\delta z = \frac{1}{g}\delta\phi = 19\ \mathrm{m}. \tag{A17}$$

REFERENCES

Bleck, R., R. Brummer, and M. A. Shapiro, 1984: Enhancement of remotely sensed temperature fields by wind observations from VHF radar network. *Mon. Wea. Rev.,* **112,** 1795–1803.

Bluestein, H. B., and D. A. Speheger, 1995: The dynamics of an upper-level trough in the baroclinic westerlies: Analysis based upon data from a wind profiler network. *Mon. Wea. Rev.,* **123,** 2369–2383.

Campistron, B., A. W. Huggins, and A. B. Long, 1991: Investigations of a winter mountain storm in Utah. Part III: Single Doppler radar measurements of turbulence. *J. Atmos. Sci.,* **48,** 1306–1318.

Carlson, C. A., and G. S. Forbes, 1989: A case study using kinematic quantities derived from a triangle of VHF Doppler wind profilers. *J. Atmos. Oceanic Technol.,* **6,** 769–778.

Cram, J. M., M. L. Kaplan, C. A. Mattocks, and J. W. Zack, 1991: The use and analysis of profiler winds to derive mesoscale height and temperature fields: Simulation and real data experiments. *Mon. Wea. Rev.,* **119,** 1040–1056.

Fankhauser, J. C., 1974: The derivation of consistent fields of wind and geopotential height from mesoscale rawinsonde data. *J. Appl. Meteor.,* **13,** 637–646.

Gal-Chen, T., 1988: A theory for the retrievals of virtual temperature from remote measurements of horizontal winds and thermal radiation. *Mon. Wea. Rev.,* **116,** 1302–1219.

Haltiner, G. J. and R. T. Williams, 1980: *Numerical Weather Prediction and Dynamic Meteorology.* John Wiley and Sons, 477 pp.

Hoehne, W. E., 1980: Precision of National Weather Service upper air measurements. NOAA Tech. Memo. NWS T&ED-16, National Weather Service, 23 pp. [NTIS PB81-108136.]

Karyampudi, V. M., M. L. Kaplan, S. E. Koch, and R. J. Zamora, 1995: The influence of the Rocky Mountains in the 13–14 April 1986 severe weather outbreak. Part I: Mesoscale lee cyclogenesis and its relationship to severe weather and dust storms. *Mon. Wea. Rev.,* **123,** 1394–1422.

Koch, S. E., M. desJardins, and P. J. Kocin, 1983: An interactive Barnes objective map analysis scheme for use with satellite and conventional data. *J. Climate Appl. Meteor.,* **22,** 1487–1503.

Kuo, Y.-H., and R. A. Anthes, 1985: Calculation of geopotential and temperature fields from an array of nearly continuous wind observations. *J. Atmos. Oceanic Technol.,* **2,** 22–34.

——, E. G. Donald, and M. A. Shapiro, 1987a: Feasibility of short range numerical weather prediction using observations from a network of profilers. *Mon. Wea. Rev.,* **115,** 2402–2427.

——, D. O. Gill, and L. Cheng 1987b: Retrieving temperature and geopotential fields from a network of wind profiler observations. *Mon. Wea. Rev.,* **115,** 3146–3165.

Locatelli, J. D., J. E. Martin, J. A. Castle, and P. V. Hobbs, 1995: Structure and evolution of winter cyclones in the central United States and their effects on the distribution of precipitation. Part III: The development of a squall line associated with weak cold frontogenesis aloft. *Mon. Wea. Rev.,* **123,** 2641–2662.

Martner, B. E., and Coauthors, 1993: An evaluation of wind profiler, RASS, and microwave radiometer performance. *Bull. Amer. Meteor. Soc.,* **74,** 599–613.

May, P. T., and R. G. Strauch, 1989: An examination of wind profiler signal processing algorithms. *J. Atmos. Oceanic Technol.,* **6,** 731–735.

Modica, G. M., and T. T. Warner, 1987: The error associated with various forms of the divergence equation to diagnose geopotential and temperatures. *Mon. Wea. Rev.,* **115,** 455–462.

Nieman, S. J., J. Schmetz, and W. P. Menzel, 1993: A comparison of several techniques to assign heights to cloud tracers. *J. Appl. Meteor.,* **32,** 1559–1568.

O'Brien, J. J., 1970: Alternative solutions to the classical vertical velocity problem. *J. Appl. Meteor.,* **9,** 197–203.

Ralph, F. M., P. J. Neiman, D. W. van de Kamp, and D. C. Law, 1995: Using spectral moment data from NOAA's 404-MHz radar wind profilers to observe precipitation. *Bull. Amer. Meteor. Soc.,* **76,** 1717–1739.

Shaltanis, D. A., 1998: Mass field retrieval using profiler data with application to low-level jet analysis. M.S. thesis, Dept. of Marine, Earth, and Atmospheric Sciences, North Carolina State University, Raleigh, NC, 157 pp.

Stankov, B. B., 1998: Multisensor retrieval of atmospheric properties. *Bull. Amer. Meteor. Soc.,* **79,** 1835–1854.

Strauch, R. G., B. C. Weber, A. S. Frisch, C. G. Little, D. A. Merritt, K. P. Moran, and P. C. Welsh, 1987: The precision and relative accuracy of profile wind measurements. *J. Atmos. Oceanic Technol.,* **4,** 563–571.

Szoke, E., J. M. Brown, J. A. McGinley, and D. Rodgers, 1994: Forecasting for a large field program: STORM-FEST. *Wea. Forecasting,* **9,** 593–605.

Trexler, C. M., and S. E. Koch, 2000: The life cycle of a mesoscale gravity wave as observed by a network of Doppler wind profilers. *Mon. Wea. Rev.,* **128,** 2423–2446.

Weber, B. L., and D. B. Wuertz, 1990: Comparison of rawinsonde and wind profile radar measurements. *J. Atmos. Oceanic Technol.,* **7,** 157–174.

Zamora, R. J., M. A. Shapiro, and C. A. Doswell III,1987: The diagnosis of upper tropospheric divergence and ageostrophic wind using profiler wind observations. *Mon. Wea. Rev.,* **115,** 871–884.

——, B. L. Weber, and D. C. Welsh, 1994: The accuracy of divergence estimates calculated using the linear vector point function method and three profilers. *Mon. Wea. Rev.,* **122,** 2603–2606.